

# ON THE EFFECT OF BUFFER LAYER SPANWISE BLOWING IN TURBULENT BOUNDARY LAYERS USING PULSED-DC PLASMA ACTUATION

A. Myers, T. C. Corke, F. O. Thomas,  
 Institute for Flow Physics and Control  
 University of Notre Dame  
 Notre Dame, IN  
 fthomas@nd.edu

## ABSTRACT

Recent active flow control experiments using pulsed-DC plasma actuation have demonstrated unprecedented levels of viscous drag reduction in turbulent boundary layers. The flow control approach involves generating a steady spanwise velocity component, on the order of the friction velocity and confined within the viscous sublayer, using an array of pulsed-DC plasma actuators. In this paper, the focus is on additional experiments that were performed to document changes in, and the recovery of, the turbulence characteristics of a canonical zero pressure gradient turbulent boundary layer associated with plasma induced spanwise blowing. Emphasis is placed on changes in coherent 3-D vortical motions associated with near-wall turbulence production that result from the spanwise blowing and the temporal response of these structures during and following termination of actuation.

## INTRODUCTION

A consensus has emerged that there is an autonomous, near-wall cycle responsible for the sustained generation of wall bounded turbulence. Versions of this mechanism are described by Jimenez and Moin (1991), Hamilton et al. (1995), Jimenez and Pinelli (1999) and Schoppa and Hussain (2002) among others. Furthermore, it is also recognized that streamwise vorticity in the turbulent boundary layer (TBL) buffer region is intimately tied to high levels of viscous drag as described by Kim (2001). These near wall longitudinal vortices serve to transfer high momentum fluid to the wall on one flank which serves to steepen the wall-normal gradient of streamwise velocity and thereby enhances friction drag. Low speed fluid is transferred away from the wall on the other flank and gives rise to the low-speed streak structure noted by Kline et al (1967) and Blackwelder and Eckelmann (1979). Our viscous drag reduction strategy is motivated by the autonomous near-wall cycle described by Schoppa and Hussain (2002). In this, the pumping action of quasi-steady streamwise vortices gives rise to the lift-up of low-speed fluid from the wall that serves to produce high levels of wall-normal vorticity,  $\omega_y$ , due to the spanwise variation in streamwise velocity,  $\partial u/\partial z$ . The magnitude of this wall-normal vorticity is a stability parameter in the ‘‘Streak Transient Growth’’ (STG) mechanism that Schoppa and Hussain (2002) link to the generation of new buffer layer streamwise vorticity. Control of the TBL involves interrupting this cycle by generating a steady spanwise velocity component,  $W \sim O(u_\tau)$ , that is confined within the sublayer. This is done by using an array of wall-mounted pulsed-DC plasma actuators as shown schematically in Figure 1. The intent is to reduce the spanwise mean flow distortion associated with the near-wall streak structure, and as a result, the wall normal vorticity component,  $\omega_y$ . This approach has led to very significant viscous drag

reduction with net power savings as reported in Thomas et al. (2019), Duong et al. (2020, 2021) and Thomas et al (2023).

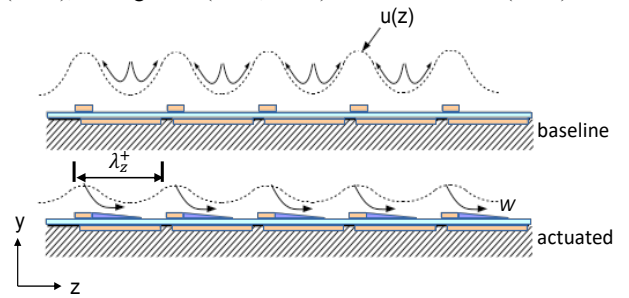


**Figure 1. Schematic of the pulsed-DC plasma induced spanwise flow that reduces wall-normal vorticity.**

In previous studies scaling relationships were obtained which showed that the drag reduction is a function of two parameters: the inner variable scaled inter-electrode spacing,  $\lambda_z^+ \equiv \lambda_z u_\tau / \nu$  and the actuator-induced spanwise velocity magnitude,  $W/u_\tau \sim O(1)$ . This scaling has allowed for the design of actuators that have produced 45% viscous drag reduction in airfoil experiments over the Mach number range of  $0.3 \leq M_\infty \leq 0.5$  (Thomas et al, 2023).

Consistent with the idea that the plasma flow control intervenes in the STG mechanism and inhibits the formation of buffer layer vortices, Duong et al (2020) utilized the quadrant splitting method of Liu and Wilmarth (1973) in a TBL at  $Re_\theta = 2,500$  to show that turbulence production associated with ejections (Q2 events) was reduced in the near wall region by 73%. Production associated with sweeps (Q4 events) was reduced by 80%. These results corresponded to a 68% reduction in viscous drag. As one would expect, this reduction in viscous drag is associated with a reduction in near-wall mean strain rate resulting from the weakened buffer layer streamwise vortices.

In this paper we report the results of experiments that were performed in order to further elucidate the flow physics associated with the introduction of a spanwise flow into the TBL buffer layer by pulsed-DC plasma actuation. In particular, focus is given to changes in and the recovery of the turbulence characteristics of a boundary layer whose viscous drag has been reduced by 62%. As in previous work, the drag reduction involves generating a steady spanwise velocity component on the order of  $u_\tau$ , within the sublayer using an array of pulsed-DC plasma actuators. The effect of this actuation on coherent 3-D vortical motions associated with near-wall turbulence and the temporal response of these structures following termination of spanwise blowing is also documented. This involves measurements of

all three velocity components in a 3-D region within the boundary layer using a pair of dual [u,v] and [u,w] hot-wire sensors during and following actuation shutoff as the boundary layer recovers to its baseline state.

### EXPERIMENTAL FACILITY AND APPROACH

All experiments were performed in the Notre Dame Low-Speed Wind Tunnel at the Hessert Laboratory for Aerospace Research. The wind tunnel is a closed-return design with turbulence management that results in free-stream turbulence levels  $\sqrt{u'^2}/U_\infty = 0.05\%$ . The test section dimensions are 0.91 m square cross-section by 2.73 m length. The freestream velocity range in the test section is from 1 m/s to 50 m/s. The test section is designed with three removable and fully interchangeable windows on all four sides. The windows can be replaced with instrumented panels that can be specifically designed for different experiments. One of these openings in the floor at the most downstream location of the test section is used to hold a floating element force balance. The force balance consisted of a recessed platen that rode on a pair of linear air bearings. The air bearings were aligned in the mean flow direction so that it was only sensitive to the streamwise component of the wall shear stress. The platen on which the plasma actuator array was mounted was adjustable at four points so that the flow-side surface of the array could be made flush to within  $\pm 0.254$  mm of the test section floor. A cantilever style load cell with a maximum rated load of 0.5 N (51 grams) was used to measure the total wall shear stress that acted over the area covered by the plasma actuator array. Two side-wall openings at the force balance location were used to mount a 3-D traversing mechanism that was used to position the [u,v] and [u,w] dual-sensor hot-wire probes. The freestream velocity was chosen such that it would provide a thick canonical turbulent boundary layer that would maximize the spatial resolution for the hot-wire probe measurements, particularly within the sublayer. These conditions are the same as those of Duong (2019) and Duong et al. (2021).

The turbulent boundary layer developed on the floor of the wind tunnel test section. The boundary layer was thickened by placing a 2-D trip strip at the entrance to the test section. This was followed by uniformly spaced 2-D roughness elements that covered the first 11% of the test section floor. The plasma actuator array was the type shown schematically in the lower portion of Figure 1 which is designed to produce a unidirectional spanwise velocity component confined to the sublayer. The spanwise spacing between the plasma actuators was  $\lambda_z = 28$  mm. In terms of the baseline TBL characteristics, this corresponded to  $\lambda_z^+ = 300$ . This spacing produced a 62% viscous drag reduction that was expected to result in tangible changes in the characteristics of the TBL that would provide insight regarding the underlying mechanisms.

The plasma actuator array mounted onto the surface of the drag force measurement platen is shown in Figure 2. The array is 22.9 cm by 22.9 cm square dimension that covered the whole surface of the platen. It consisted of 7 plasma actuators connected in parallel to the pulsed-DC power source. The electrodes consisted of 0.106 mm thick copper foil tape. In the photograph, the exposed electrodes are the narrow strips aligned in the flow direction. The covered electrodes are the wider copper strips with one each per exposed electrode. These appear as a dull copper color because they are being viewed through the translucent 0.1016 mm thick sheet of V2-quality muscovite mica dielectric material. The underside of the mica was backed by a 0.0254 mm thick sheet of Kapton. The complete plasma actuator array was bonded to a 25.4 mm thick Garolite sheet that was subsequently mounted to the force balance that was used to directly measure

the viscous drag on the surface covered by the plasma actuator array.

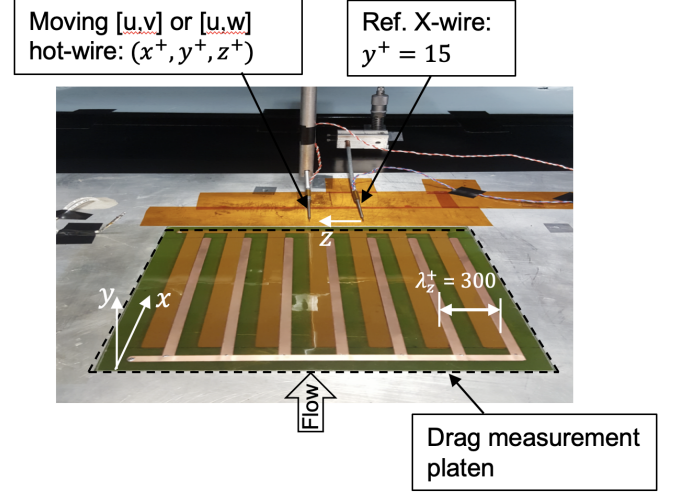


**Figure 2. Photograph showing plasma actuator array mounted onto the surface of the drag measurement platen, reference X wire probe and movable pair of X hot-wire probes.**

The setup included a single [u,v] dual-sensor hot-wire that was fixed in space at a location that was 1 cm, or  $x^+ = 115$  downstream of the actuator array. The spanwise location of the fixed sensor aligned with the edge of an exposed electrode of one of the plasma actuators in the array. This spanwise location of the fixed [u,v] sensor is defined as  $z = 0$ . The wall-normal position of the fixed [u, v] sensor corresponded to  $y^+ = 15$ . The second sensor involved interchangeable [u,v] and [u,w] hot-wires that were mounted to the traversing mechanism and moved in 3-D space throughout the boundary layer. All of the hot-wires were operated in a constant temperature mode using a specially designed circuit that allowed the reference ground to float. This was essential for the hot-wire sensors to allow them to be placed in the weakly ionized air stream directly downstream of and directly over the plasma actuator array. Details of the anemometer circuit are provided in Duong (2019). The voltage time series from the dual sensor hot-wire probes was analog frequency compensated to 8 kHz and anti-alias filtered at 10 kHz before being simultaneously digitally sampled at 20 kHz. The voltage time series were converted to velocity time series through the application of previously determined voltage-velocity calibrations for each hot-wire sensor.

### RESULTS

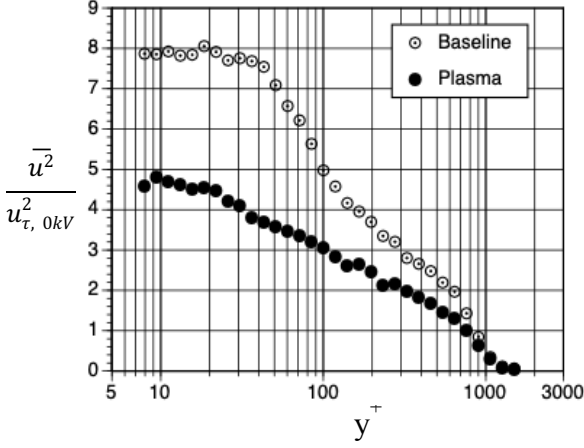
In this section, sample results are presented for buffer layer spanwise blowing by pulsed-DC plasma actuation in an approach zero pressure gradient TBL under the conditions shown in Table 1.

Table 1. Experimental Parameters.

$U_\infty$ (m/s)	$Re_\theta$	$Re_\tau$	$\delta$ (mm)	$u_\tau$ (m/s)
4.6	2,500	1,525	140	0.17

Figure 3 compares wall-normal profiles of streamwise component turbulent normal stress obtained at spanwise location  $z^+ = 50$  for the baseline and actuated TBL. This serves as an

example of the significant reduction of turbulence stress resulting from the plasma actuation. As expected, the reduction is greatest in the near-wall region but extends throughout most of the boundary layer. A spanwise sequence of profile measurements presented in Myers (2023) shows that the turbulent stress reduction shown below did not vary with span.



**Figure 3. Streamwise component turbulent normal-stress reduction due to plasma-induced spanwise flow.**

Figure 4 compares wall-normal profiles of outer variable scaled turbulence production,

$$P \equiv -\overline{uv} (d\overline{U}/dy) (\delta/U_\infty^3) \quad (1)$$

for the baseline and plasma actuated turbulent boundary layers. These data were also obtained at  $z^+ = 50$  but the results were also largely spanwise invariant. This figure shows a 66 % peak reduction in turbulence production at  $y^+ = 12$ . Although not presented here, quadrant splitting measurements presented in Myers (2023) show a 52% reduction in production associated with ejection (Q2) events and a 48% reduction for sweep (Q4) events.

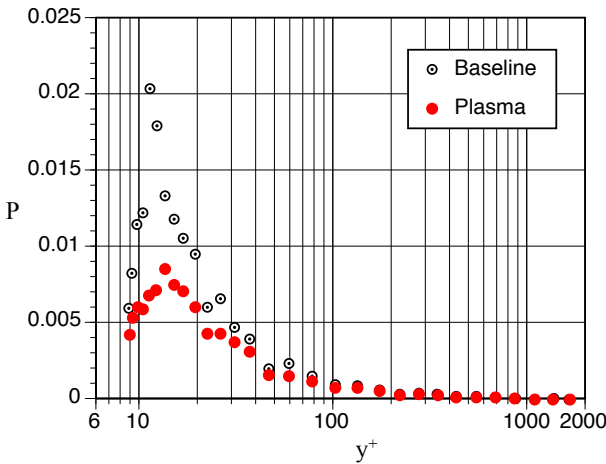


**Figure 4. Comparison of wall normal profiles of outer-variable scaled turbulence production, P, for the baseline and plasma actuated TBLs.**

### Conditional Measurements

In order to further investigate the effect of the flow control on the coherent structures in the near-wall region of the boundary layer, conditional-averaged reconstructions of relevant flow field quantities were performed. For this, the X hot-wire

probe at the fixed  $[x, z]$  location remained positioned at  $y^+ = 15$ . The fixed probe provided the  $[u, v]$  time series used to define “events” on which the conditional averages would be based. The other  $[u, v]$  and  $[u, w]$  sensing hot-wire probes were located at the same  $x$  location as the fixed probe, but were moved in the  $[y, z]$  plane. The time series from both the fixed and moving hot-wire probes were sampled simultaneously.

The method for defining an “event” utilized the “Variable-Interval Time-Averaged” (VITA) technique that was pioneered by Blackwelder and Kaplan (1976). This utilized the  $u$  velocity time series at the fixed probe and applied a discriminator function,  $D(t)$ , such that,

$$D(t) = \begin{cases} 1 & \text{if } \widehat{v\hat{a}r} > k u_{rms}^2 \\ 0 & \text{otherwise} \end{cases} \quad (2)$$

where,

$$\widehat{v\hat{a}r}(x_i, t, T) = \widehat{u^2}(x_i, t, T) - [u(x_i, t, T)]^2$$

is the localized variance of streamwise velocity fluctuations over the time interval  $T$  at a spatial location,  $x_i$ . With this discriminator,  $k=1.2$  and  $T u_\tau^2/\nu=10$  which are the Blackwelder and Kaplan (1976) recommended values. Once a reference time for each VITA event was determined by the detection function,  $D(t)$ , a conditional average of a given flow quantity,  $q$ , in time and space was constructed based on,

$$\langle q(y_i, z_i, T) \rangle_{y^+=15} = \frac{1}{N} \sum_j^N q(y_i, z_i, t_j + T) \quad (3)$$

Since  $D(t)$  was equal to unity only during very short time intervals, the times  $t_j$  were taken to be midway between the beginning and end of the period during which  $D(t) \neq 0$ . A positive or negative time delay  $T^*$  with a range  $-4 \leq T^* = TU_\infty/\delta \leq 4$  was applied to determine the temporal behavior of a given quantity before and after a detection occurred.

In constructing a 3-D representation of the coherent vortical structures, it was important to determine the spanwise extent over which detected events were correlated. This was based upon the correlation coefficient,  $[R(z^+, \tau)]_{\max}$ , between events detected at the fixed probe to that detected at the moving probe. Both probes were located at  $y^+ = 15$ . The spanwise range of the moving probe was  $50 \leq z^+ \leq 600$ . The results showed a reasonable spanwise spatial correlation, prior to a sharp drop off that commenced at  $z^+ = 400$ . This was then taken as the spanwise limit over which flow reconstructions were considered valid.

The method of flow control is based on active intervention in STG and for which the level of wall normal vorticity,  $\omega_y$ , is a critical stability parameter. To investigate this, Figure 5 compares  $\langle \omega_y(y^+ = 15, z_i^+, x_i^+) \rangle_{y^+=15}$  for the baseline and drag-reduced boundary layers. For Figure 5 and the plots to follow, the dimensionless time scale,  $T^* = TU_\infty/\delta$ , was converted to a dimensionless pseudo-spatial streamwise length scale,  $x^+$ , assuming a convection speed of  $0.6U_\infty$ .  $x^+ = 0$  corresponds to the time of the VITA detection and the equivalent flow direction is from left to right. Figure 6 reveals a significant reduction of  $\omega_y$  in the drag-reduced boundary layer. When averaged over a 3-D near-wall region given by,  $0 \leq y^+ \leq 20$  by  $-250 \leq x^+ \leq 250$  by  $0 \leq z^+ \leq 400$ , in the actuated boundary layer the spatially averaged wall normal vorticity is reduced by 60% compared to the baseline boundary layer.

Intervention in the autonomous STG cycle by reduction of  $\omega_y$  should have the effect of reducing near-wall streamwise vorticity,  $\omega_x$ . To investigate this effect, color-mapped levels of conditionally averaged values of  $\langle \omega_x(y^+ = 15, z_i^+, x_i^+) \rangle_{y^+=15}$  are presented for the baseline and drag-reduced boundary layers in Figure 6. The coherent features for the baseline boundary

layer are consistent with the presence of longitudinal vortical structures associated with the wall streak structure. The

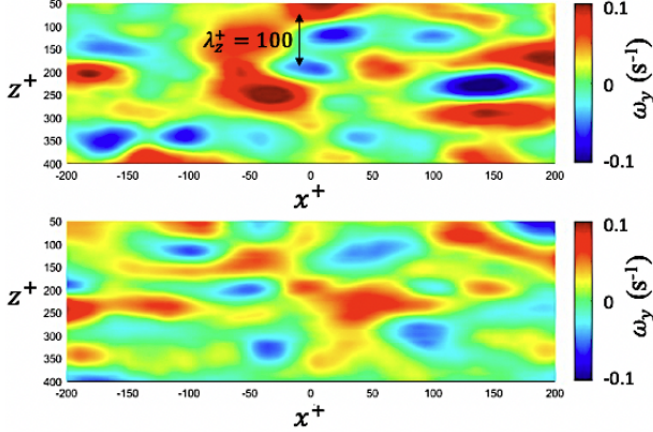


**Figure 5. Iso-surfaces of  $\langle \omega_y(y^+ = 15, z_i^+, x_i^+) \rangle_{y^+=15}$  for the baseline boundary layer (top) and drag-reduced boundary layer (bottom).**

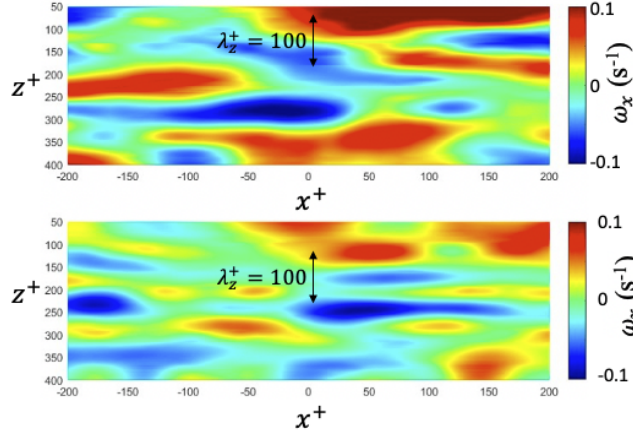


**Figure 6. Iso-surfaces of  $\langle \omega_x(y^+ = 15, z_i^+, x_i^+) \rangle_{y^+=15}$  baseline boundary layer (top) and drag-reduced boundary layer (bottom).**

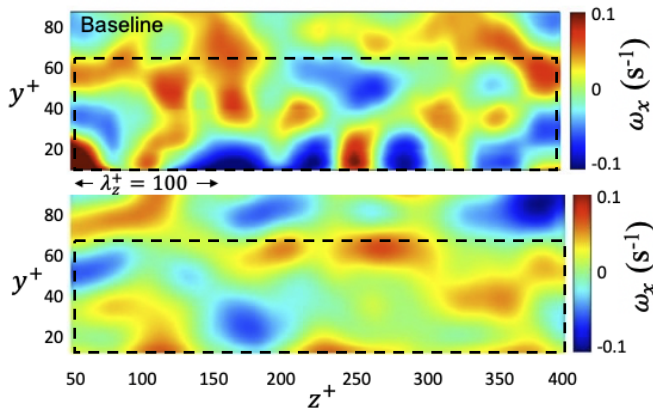


**Figure 7. Iso-surfaces of  $\langle \omega_x(y_i^+, z_i^+, TZ = 0) \rangle_{y^+=15}$  for the baseline boundary layer (top) and drag-reduced boundary layer (bottom).**

denoted spanwise wavelength of  $\lambda_z^+ = 100$  is consistent with the average low-speed streak spanwise wavelength. Compared to the baseline boundary layer, the  $\omega_x$  levels are clearly reduced in the plasma actuated boundary layer as is their streamwise extent (i.e. duration). However, when normalized by the lower  $u_\tau$  of this case, the spanwise wavelength scaling of the elongated vortical structures remains at  $\lambda_z^+ = 100$ .

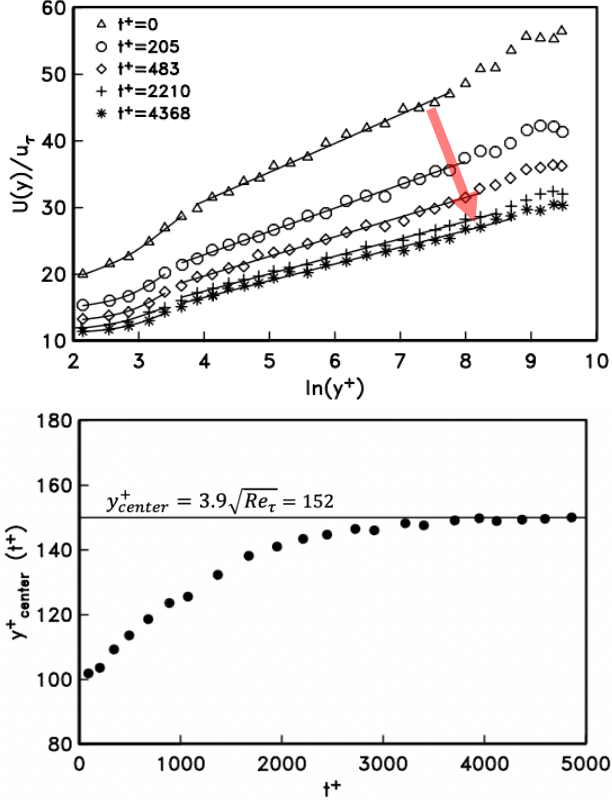
Figure 7 compares color-mapped levels of streamwise vorticity  $\langle \omega_x(y_i^+, z_i^+, T = 0) \rangle_{y^+=15}$  for the baseline and plasma actuated boundary layers. This represents a cut in the  $[y, z]$ -cross flow plane at  $x^+ = 0$  of the streamwise vorticity contours shown previously at  $y^+ = 15$  in Figure 6. The cross-flow plane view of  $\omega_x$  for the baseline boundary layer reveals near-wall counter-rotating ( $\pm\omega_x$ ) vortex pairs with an average spacing of  $\lambda_z^+ = 100$  that is consistent with the low speed streak structure (Kline et al. 1967). For the plasma-actuated boundary layer, the  $[x, z]$  plane view of  $\omega_x$  reveals a dramatic decrease in the streamwise vorticity magnitude compared to the baseline boundary layer, particularly in the region  $y^+ \leq 60$  (as highlighted by the dashed lines). Again, accounting for the resulting lower friction velocity, the spacing of the structures in the drag reduced boundary layer retains the same  $\lambda_z^+ = 100$ .

#### Temporal Recovery of Baseline TBL Characteristics

A timing circuit described in Myers (2023) was used to document temporal changes in the TBL as it returned to its baseline state following termination of plasma flow control. The actuation was terminated after 10 seconds of operation, corresponding to a  $t_1^+ = 18,525$  (far longer than the time required to reach full 62% drag reduction ( $\Delta t^+ \sim O(200)$ ) as suggested in Duong et al (2021). The velocity time series recorded by the hot-wires was continued for an additional 20 seconds, corresponding to  $t_2^+ = 37,050$ , which was found to be of sufficient duration for the boundary layer conditions (both mean and fluctuating) to reach the asymptotic baseline state.

Figure 8 (top) shows the boundary layer mean streamwise velocity profile normalized using inner variables at seven dimensionless times,  $t^+ = t u_\tau^2 / \nu$  after termination of the actuation where instantaneous values of  $u_\tau(t)$  have been used in the scaling. The corresponding temporal development of the location of the geometric center of the log region (Mathis et al , 2009) is shown in the bottom part of Figure 8. These indicate that following termination of the spanwise blowing, the mean profile asymptotes to its baseline state, in  $t^+ \approx 3,200$ . If the scaling is performed using the baseline value of  $u_\tau$  the recovery time is somewhat longer,  $t^+ \approx 4,000$ .

Figure 9a presents the temporal evolution of the root-mean-square fluctuation levels of the three components of fluctuating velocity,  $u_{i,rms}$ , as the boundary layer returns to its nominal state following termination of actuation. The values are normalized by the corresponding baseline TBL values. These appear to reach 99% of the nominal baseline fluctuation levels by  $t^+ \approx 4000$  (again based on the instantaneous value of  $u_\tau(t)$ ) which is somewhat later than the mean flow.



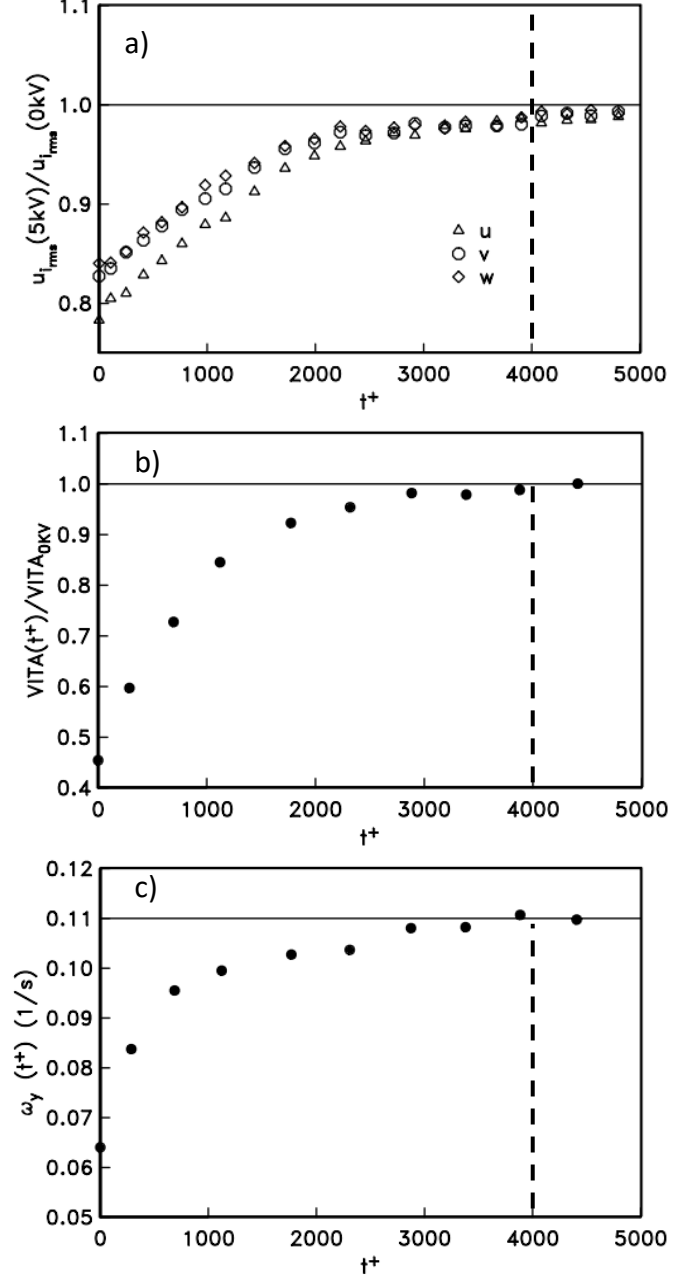
**Figure 8. Temporal recovery of the inner-variable-scaled mean streamwise velocity profiles (top) and log profile geometric center location (bottom) following the termination of the plasma drag reduction occurring at  $t^+ = 0$ . Note that the indicated  $t^+$  values account for  $u_\tau(t)$ .**

Figure 9b presents the temporal evolution of the frequency of VITA events (normalized by the baseline TBL value) after termination of actuation at  $t^+ = 0$ . The VITA events are associated with the instability of near-wall streaks and turbulence production. The temporal evolution of VITA frequency in Figure 9b is shown to be strongly correlated with the  $u_{i,rms}$  recovery shown in Figure 9a.

Recall that our flow control approach is based on the concept that “streak transient growth” depends critically on the magnitude of  $\omega_y$  which the plasma-induced spanwise flow is designed to reduce. Figure 9c presents the temporal evolution of the value of *spatially averaged*  $\omega_y$  over a 3-D wall region given by,  $0 \leq y^+ \leq 20$  by  $-250 \leq x^+ \leq 250$  by  $0 \leq z^+ \leq 400$ . Figure 9c indicates a relatively smooth increase in  $\omega_y$  upon termination of the spanwise blowing. This, in turn, has been shown to be associated with the redevelopment of streamwise buffer layer vortices. Note that the temporal evolution of  $\omega_y$  in Figure 9c is fully consistent with the temporal evolution of both the frequency of VITA events and the turbulence root-mean-square levels of the three fluctuating velocity components.

## CONCLUSION

Experiments were performed using an active flow control approach that involves generating a steady spanwise velocity component on the order of  $u_\tau$ , within the TBL sublayer using an array of pulsed-DC plasma actuators. This has shown the ability to significantly reduce the viscous drag in turbulent boundary



**Figure 9. Temporal evolution of: (a) the  $u_{rms}, v_{rms}, w_{rms}$  levels measured at  $y^+ = 15$  normalized by their respective baseline values, (b) the normalized VITA event frequency measured at  $y^+ = 15$ , (c) spatially averaged wall-normal vorticity,  $\omega_y$ . Note that in each case  $t^+$  accounts for the temporal variation of  $u_\tau(t)$ .**

layers. The intent is to reduce the wall normal vorticity component,  $\omega_y$ , that is associated with the spanwise mean flow distortion caused by streamwise buffer layer vorticity. The significance of the  $\omega_y$  comes from Schoppa and Hussain’s (2002) proposed STG mechanism for the self-sustained generation of new buffer layer vorticity and which Kim (2001) and others have linked to skin friction drag. Conditional averages were used to reconstruct the 3-D coherent motions associated with the occurrence of VITA events. These events were found to be correlated in the spanwise direction out to  $z^+ = 400$  that defined the spanwise extent of the spatial

reconstructions. The results presented here compare the characteristics of a baseline turbulent boundary layer to those in which the viscous drag was reduced by 62%.

Comparison of conditional flow field reconstructions of wall-normal vorticity in the baseline and actuated TBLs reveals a significant reduction in  $\omega_y$  in the drag-reduced boundary layer. This is due to the plasma imposed spanwise buffer layer flow reducing the spanwise velocity gradient  $\partial u/\partial z$  associated with the wall streak structure. In fact, when averaged over a 3-D near-wall region in the drag-reduced boundary layer, the spatially averaged  $\omega_y$  was reduced by 60% compared to the baseline case. As a consequence of inhibiting STG, the near-wall streamwise vorticity in the actuated boundary layer also reveals a very significant decrease relative to the baseline case which is particularly apparent in the region  $y^+ \leq 60$  (Fig. 7).

Regarding the conditional measurements, it is important to remember that both the baseline and plasma actuated cases are based on the occurrence of turbulence producing VITA events. In this sense, although the disparity between the presented cases is very significant (e.g. Figures 5, 6, 7) this represents a “worst case scenario” because the plasma actuated case excludes those quiescent periods when VITA events are fully suppressed by the spanwise buffer layer flow.

Upon termination of the plasma-induced buffer layer flow, the mean boundary layer profile based on the temporal evolution of the geometric center of the log region, was found to return to its nominal state in  $t^+ \approx 3200$ . This value accounts for the time-variation of  $u_\tau(t)$ . If the baseline value of  $u_\tau$  is used the scaled recovery time is somewhat longer,  $t^+ \approx 4,000$ . The turbulence root-mean square level of all three velocity components reached within 99% of their respective nominal baseline values at  $t^+ \approx 4,000$  again accounting for the temporal variation of  $u_\tau(t)$ . Thus, the recovery of the mean flow is found to slightly precede the turbulent stresses, as one might well expect. Of particular interest is the comparison of the temporal recovery of turbulent stresses, the relative frequency of VITA events and the spatial average value of wall normal vorticity shown in Figure 9. The temporal variation of the the frequency of VITA ejection-sweep events and volume averaged wall normal vorticity are shown to perfectly track that of the recovering turbulence stresses which is fully consistent with what one would expect based on the STG mechanism. The wall normal vorticity needs to reach a critical value for the STG mechanism to give rise to the creation of new buffer layer longitudinal vortices which are key in near wall turbulence production. Given that the wall-normal vorticity shown in Figure 9c is spatially averaged, this likely accounts for the smooth temporal variation although it should also be noted that the temporal gradient near  $t^+=0$  is quite large.

The 99% wall shear stress recovery after termination of the actuation occurs within  $t^+=4000$  (based on the baseline values of  $u_\tau$ ). If one assumes a convective speed of  $U_c \approx 0.6 U_\infty$  the corresponding streamwise distance for shear stress recovery becomes  $x^+ = U_c^+ t^+ \approx 65,000$ . This, in turn, corresponds to a streamwise fetch of  $x/\delta \approx 43$ . Such a value certainly does not suggest a direct coupling with the outer flow in terms of giving rise to the resumption of near-wall turbulence production.

Finally, to relate the VITA event frequency to the friction velocity (i.e. wall shear stress), in Figure 10 it is shown that the increase in the relative frequency of VITA events at  $y^+ = 15$  during the period that follows the termination of the plasma induced spanwise blowing is in direct proportion to the increase in friction velocity  $u_\tau(t^+)$  as it returns back to its higher baseline state.

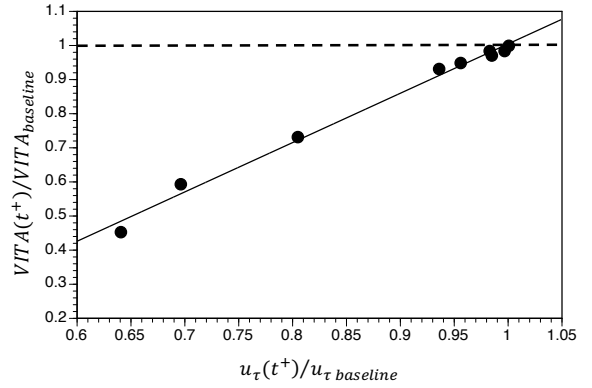


**Figure 10. Linear correlation between of the normalized VITA event frequencies measured at  $y^+ = 15$  and the friction velocity, following the termination of actuation at  $t^+ = 0$ .**

## REFERENCES

- R. Blackwelder and R. Kaplan. On the wall structure of the turbulent boundary layer. *J. Fluid Mech.*, 76(1):89–112, 1976.
- A. Duong, S. Midya, T. Corke, F. Hussain, and F. Thomas. Turbulent boundary layer drag reduction using pulsed-dc plasma actuation. *Proceedings of the 11th International Symposium on Turbulence and Shear Flow Phenomena*, Southampton, UK, 2019.
- A. Duong, T. Corke, and F. Thomas. Characteristics of drag reduced turbulent boundary layers through pulsed-dc plasma actuation. *AIAA Paper 2020-0098*, January 2020.
- A. Duong, T. Corke, and F. Thomas. Characteristics of drag-reduced turbulent boundary layers with pulsed-direct-current plasma actuation. *J. Fluid Mech.*, 915(A113):1–29, 2021.
- J. Hamilton, J. Kim, and F. Waleffe. Regeneration mechanisms of turbulence near wall structure. *J. Fluid Mech.*, 287:317–489, 1995.
- J. Jimenez and P. Moin. The minimal flow unit in near wall turbulence. *J. Fluid Mech.*, 225: 213–240, 1991.
- J. Jimenez and A. Pinelli. The autonomous cycle of near-wall turbulence. *J. Fluid Mechanics*, 389:335–359, 1999.
- J. Kim. Physics and control of wall turbulence for drag reduction. *Phil. Trans. R. Soc. A*, 369: 1396–1411, 2001.
- S. Kline, W. Reynolds, F. Schraub, and P. Runstadler. The structure of turbulent boundary layers. *J. Fluid Mech.*, 30:741–773, 1967a.
- R. Mathis, N. Hutchins, and I. Marusic. Large-scale amplitude modulation of small-scale structures in turbulent boundary layers. *J. Fluid Mech.*, 628:311–337, June 2009.
- A. Meyers. Active boundary layer control: An experimental investigation in turbulent boundary layer skin-friction drag reduction using pulsed dc plasma actuator. Ph.D. Thesis, University of Notre Dame, July 2023.
- W. Schoppa and F. Hussain. Coherent structure generation on near-wall turbulence. *J. Fluid Mech.*, 453:57–108, 2002.
- F. Thomas, T. Corke, A. Duong, S. Midya, and K. Yates. Turbulent drag reduction using pulsed-dc plasma actuation. *J. Phys. D: Appl. Phys.*, 52, 2019.
- F. Thomas, T. Corke, and A. Duong. “Airfoil friction drag reduction with net power savings using pulsed-direct-current plasma actuation”, *AIAA J.*, 61(9):4045–4055, 2023.